journal of the mechanical behavior of biomedical materials 131 (2022) 105249

Contents lists available at ScienceDirect

Journal of the Mechanical Behavior of Biomedical Materials

journal homepage: www.elsevier.com/locate/jmbbm

Research paper

In-plane and out-of-plane deformations of gilt utero-sacral ligaments

Kandace Donaldson [a], Joseph Thomas [b], Yizheng Zhu [b], Sherrie Clark-Deener [c], Marianna Alperin [d], Raffaella De Vita [a,*]

[a] Department of Biomedical Engineering and Mechanics, Virginia Tech, 330A Kelly Hall, 325 Stanger Street, Blacksburg, VA, 24061, USA
[b] Department of Electrical and Computer Engineering, Virginia Tech, 460 Turner Street, Suite 303, Blacksburg, VA, 24061, USA
[c] Department of Large Animal Clinical Sciences, Virginia Tech, 215 Duckpond Drive, Blacksburg, VA, 24061, USA
[d] Department of Obstetrics, Gynecology & Reproductive Sciences, Division of Female Medicine and Reconstructive Surgery, University of California San Diego, 9500 Gilman Drive, La Jolla, CA, 92093, USA

ARTICLE INFO

Keywords:
Uterosacral ligaments
Pelvic floor support
Biaxial testing
Deformations
Digital image correlation
Optical coherence tomography

ABSTRACT

The uterosacral ligaments (USLs) are supportive structures of the uterus and apical vagina. The mechanical function of these ligaments within the pelvic floor is crucial not only in normal physiological conditions but also in reconstructive surgeries for pelvic organ prolapse. Discrepancies in their anatomical and histological description exist in the literature, but such discrepancies are likely due to large variations of these structures. This makes mechanical testing very challenging, requiring the development of advanced methods for characterizing their mechanical properties. This study proposes the use of planar biaxial testing, digital image correlation (DIC), and optical coherence tomography (OCT) to quantify the deformations of the USLs, both in-plane and out-of-plane. Using the gilts as an animal model, the USLs were found to deform significantly less in their main direction (MD) of *in vivo* loading than in the direction perpendicular to it (PD) at increasing equibiaxial stresses. Under constant equibiaxial loading, the USLs deform over time equally, at comparable rates in both the MD and PD. The thickness of the USLs decreases as the equibiaxial loading increases but, under constant equibiaxial loading, the thickness increases in some specimens and decreases in others. These findings could contribute to the design of new mesh materials that augment the support function of USLs as well as noninvasive diagnostic tools for evaluating the integrity of the USLs.

1. Introduction

Pelvic organ prolapse (POP) is a serious problem that results in physical, mental, and emotional pain for many women and others with female anatomy. This disorder is estimated to affect up to 50% of women in the U.S. with numbers increasing every year as a sizable share of the population ages (Wu et al., 2009; Barber and Maher, 2013b). Treatment options for POP are limited; conservative treatments include physical therapy and pessaries that hold up the prolapsed organs while more direct treatments involve surgery. Inconsistency between pre-surgical *versus* intra-operative measurement of prolapse makes planning surgery difficult (Vineyard et al., 2002; Vierhout et al., 2006; Fayyad et al., 2007; Chao et al., 2012; Doumouchtsis et al., 2017). It is estimated that 12.6% of women in the U.S. will undergo surgery to correct POP in their lifetimes (Wu et al., 2014). Increased scrutiny of transvaginal meshes have raised interest in using native tissues to restore support to the pelvic organs (Diwadkar et al., 2009; Skoczylas et al., 2014; Holt, 2019).

The uterosacral ligaments (USLs), as the main support structures for the uterus and apical vagina, are often targeted for POP reconstructive surgeries. In such surgeries, either the vaginal vault or the uterus is affixed to the USLs with sutures, restoring support to the prolapsed organs, likely increasing tension on the USLs. Though USL suspension surgeries generally have high rates of success (in the 80%+ range), complications, recurrence of prolapse, and necessity of additional surgeries are not uncommon (Barber et al., 2000; Margulies et al., 2010; Barber and Maher, 2013a; Turner et al., 2016). To improve surgical outcomes for POP, surgical materials and procedures must be developed which account for the complex mechanical realities of the pelvic support tissues. For this, a thorough and nuanced understanding of the USLs' mechanical role in pelvic organ support must be developed.

The USLs, though referred to as 'ligaments', are very different from the fibrous articular ligaments. They are membrane-like and heterogeneous, comprised mainly of collagen with smooth muscle, nerve fibers, blood vessels, lymphatics, and adipose tissue. Their primary axis of mechanical support stretches from the sacral spine/sacrospinous

* Corresponding author.
E-mail address: devita@vt.edu (R. De Vita).

https://doi.org/10.1016/j.jmbbm.2022.105249
Received 13 January 2022; Received in revised form 7 April 2022; Accepted 17 April 2022
Available online 25 April 2022

ligament/coccygeous distally to the cervix, but they form a contiguous network of soft supportive tissues including the cardinal ligaments and other more nebulous connective tissue (Campbell, 1950). A key characteristic of the USLs is their variability, both along their length and between different individuals. Studies show that different patients' USLs can vary in their size as well as which sacral vertebrae they attach to (Buller et al., 2001; Umek et al., 2004; Siddique et al., 2006; Vu et al., 2010; Ramanah et al., 2012). Within the structure of each USL, the composition varies between the proximal and distal regions. The distal region of the USLs abutting the cervix/vagina is primarily composed of smooth muscle while the proximal region contains mainly collagen and looser connective tissue, with a gradient of collagen and smooth muscle spanning the attachment sites (Campbell, 1950). Accordingly, the USLs are generally considered in terms of three distinct regions, arbitrarily defined as equal thirds: the distal/cervical region, the intermediate region, and the proximal/sacral region. Most mechanical studies of the USLs do not account for the variability in their structure. For example, Danso et al. (2020) recently compared the biaxial tensile properties of human USLs from patients with and without POP. However, since the USLs were obtained from patients during pelvic surgery, only specimens from the most distal portions of the USLs were isolated and tested in order to avoid inflicting undue harm, thus highlighting the usefulness of animal studies.

The highly complex anatomical and mechanical reality of the *in vivo* USLs is difficult to replicate in *ex vivo* experiments. A thorough review of published studies has recently been published by Donaldson et al. (2021). To characterize the mechanical properties of the USLs with as much anatomical relevancy as possible, several studies have employed planar biaxial testing coupled with digital image correlation (DIC). The DIC is an optical full-field strain mapping technique in which the movement of applied patterns on the surface of specimens is tracked by cameras. The in-plane displacements of such patterns are then obtained and the strains are calculated (Sutton et al., 2009). Using this technique, Becker and De Vita (2015) and Tan et al. (2016) investigated the elastic and viscoelastic properties of a tissue complex comprised of USL and cardinal ligament from sows, or swine that have given birth. These studies found some potential material anisotropy, with the tissues being stiffer and deforming less in the main *in vivo* loading direction (MD) (i.e., the direction from the cervix to the sacrum which experiences the largest gravitational loads), compared to the direction perpendicular to it (PD). These results were supported by previous findings by Baah-Dwomoh et al. (2016) who tested specimens isolated from the distal swine USLs, although these authors did not report a statistically significant difference between the mechanical properties in the MD and PD. The study by Baah-Dwomoh et al. (2016) also found that the sow USLs were very similar to the human USLs in terms of histology, elastic properties, and viscoelastic properties. More recently, Pack et al. (2020) tested the elasticity of the distal region of USLs from gilts (virgin swine) using similar methods, finding no difference in secant moduli between the two loading directions. No past studies have characterized the time-dependent deformations of the USLs under constant loading, or creep response, in gilts.

Given their membrane-like structure, the through-thickness deformations of the USLs can be studied using optical coherence tomography (OCT), a noninvasive imaging modality that provides high resolution, cross-sectional imaging of tissues by measuring the time of flight for backscattered light (Huang et al., 1991). Most tissues can be penetrated optically up to a few millimeters of depth, especially at near-infrared regions where the absorption of light is low (Fercher et al., 2003). The internal morphology of the tissues can thus be visualized and quantified with micrometer resolution. Since its introduction in 1991, OCT has been most widely used in ophthalmology for imaging the retina and anterior segment of the eye (Drexler and Fujimoto, 2008). It has also received significant interest in endoscopy for cardiovascular and gastrointestinal systems, among many other applications (Bouma et al., 2000; Jang et al., 2005; Adhi and Duker, 2013). In biomechanics, OCT-based elastography has been used to measure quantities such as strain, elastic modulus, and stiffness of soft tissues (Huang et al., 2009; Sun et al., 2013; Larin and Sampson, 2017; Sun et al., 2011), but studies on creep remain rare (Matveev et al., 2017). To the best of our knowledge, OCT has never been applied to analyze the through-thickness of the USLs during mechanical testing.

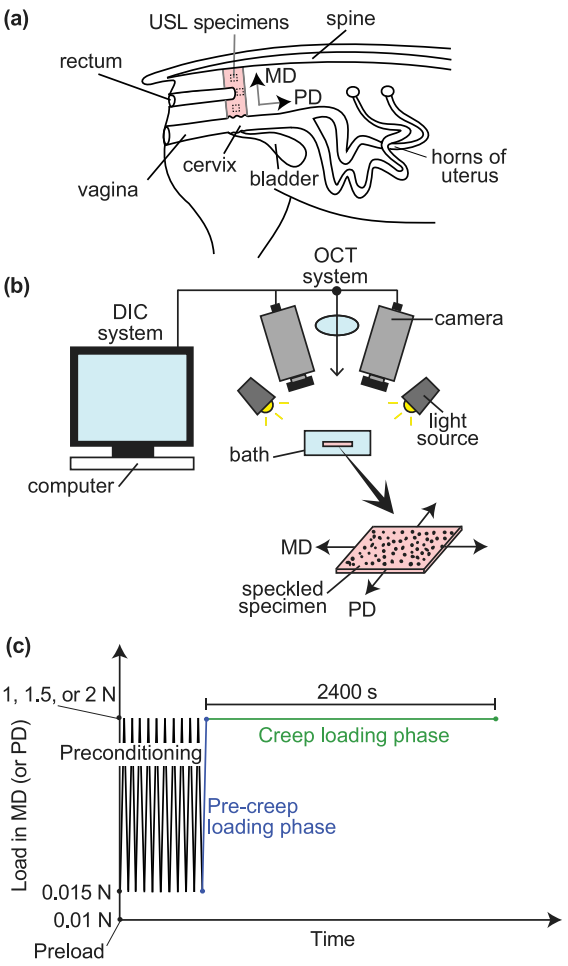

Fig. 1. (a) Location of USL specimens in the gilt with main direction (MD) and perpendicular direction (PD). (b) Experimental equipment including a custom-made biaxial machine, digital image correlation (DIC) system, and optical coherence tomography (OCT) system. (c) Testing protocol showing the loading profile over time in the MD (or PD).

In this study, we quantify the in-plane and out-of-plane deformations of the USLs from gilts and explore differences of in-plane strains between the main physiological loading direction of the USLs and the complementary direction. To account for the highly heterogeneous and variable morphology of the USLs, we use planar biaxial testing in combination with DIC and OCT methods. The results could lead to a better understanding of the complex and variable behavior of the USLs, which is necessary for the development of biocompatible surgical materials that are functionally similar to the USLs. Additionally, this research may contribute to the creation of tools to improve surgical planning for USL suspension procedures.

2. Materials and methods

2.1. Specimen preparation

This study was conducted with approval from the Institutional Animal Care and Use Committee (IACUC) at Virginia Tech. A total of

5 gilts (virgin swine), aged 6–8 months and weighing 300–350 lbs, were used for this study. The gilts were anaesthetized and sacrificed by injection of phenytoin/pentobarbital solution. Following sacrifice, the distal, intermediate, and sometimes the proximal portions of the USLs were excised and stored at −20 °C. Prior to mechanical testing, the USLs were thawed, and square specimens of approximately 15 × 15 mm^2 were cut with their sides aligned with the MD and the PD (Fig. 1(a)). A quick-drying matte black spray paint was applied through a mesh screen to create a speckle pattern on the surface of the specimens for non-contact strain measurements. The specimens were held under gentle airflow using a laboratory compressed air tap for 5–10 s before and after speckling for better adhesion. Once the paint was dry, the specimens were hydrated with phosphate-buffered saline (PBS, pH 7.4, DOT Scientific Inc., Burton, MI) and mounted on four custom-made 3D printed clamps, each with three L-shaped needles, spaced 3.5 mm, for puncturing the tissue along each side using the tissue clamping setup previously described by Huntington et al. (2021).

2.2. Mechanical testing

A total of 15 specimens were equibiaxially tested, one specimen from each of three gilts, five specimens from one gilt, and seven specimens from the remaining gilt. Of these, seven specimens came from right-side USLs, and eight specimens came from left-side USLs. Following specimen preparation, the tissues were loaded into a custom-built biaxial tensile testing apparatus consisting of two load cells of 8.9 N-capacity and 0.1% accuracy (FSH00092, Futek Advanced Sensor Technology, Inc., Irvine, CA), four linear actuators (T-NA08A25, Zaber Technologies, Inc., Vancouver, BC, Canada) with a micro-step size resolution of 0.048 μm and maximum travel length of 25 mm, and an acrylic bath filled with room-temperature PBS (Fig. 1(b)). All testing protocols were programmed in LabVIEW (NI, Austin, TX).

Specimens were biaxially preloaded to 0.01 N at a displacement rate of 3 μm/s (Fig. 1(c)). This displacement rate was selected due to its use in mechanical testing of other pelvic tissue specimens of comparable size using the same apparatus (Huntington et al., 2019). Once the tissue reached the target load of 0.01 N along both loading axes, the specimens were preconditioned by subjecting them to ten loading/unloading cycles between 0.015 N and an upper load of 1, 1.5, or 2 N at a displacement rate of 5 μm/s. The rate during preconditioning was slightly faster than the rate used for preload in order to reduce the time it took to reach the creep load while remaining quasi-static. Due to the considerable heterogeneity of the USL tissue specimens, several preliminary tests failed by tissue delamination or tearing. Because of the variation in tissue quality, the maximum load during the pre-creep phase (or the creep load) had to be lowered from the initial selection of 2 N to 1.5 N and finally to 1 N in order to maintain the tissues' integrity. Of the 15 total tested specimens, three were loaded up to 2 N, three were loaded up to 1.5 N, and nine were loaded up to 1 N, and they were kept at such loads during creep for 40 min. The time interval for creep was chosen to be larger than the time interval used in a previous study which showed that the largest increase in strain for swine USL/cardinal ligament complexes occurred in the first 20 min (Tan et al., 2016).

2.3. DIC imaging and in-plane deformations

For all strain measurements, the undeformed original configuration was considered to be that at the preload of 0.01 N. High-resolution (2448 × 2048 pixels) images were continuously taken using two CMOS cameras (Basler ace acA2440-75 μm, Basler, Inc., Exton, PA) from different angles at 1 Hz. The cameras were focused on the specimens prior to testing, and the DIC system was calibrated using a standard calibration grid with 3 mm spacing. Post-processing of the collected images was performed using a commercial 3D DIC system (Vic-3D, version 9, Correlated Solutions Inc., Irmo, SC).

Axial Lagrangian strains in the two loading directions were calculated over a region of interest of approximately 5 × 5 mm^2 in the center of the specimens. The average was taken over the selected region for each image, yielding mean values of strain at each second during the pre-creep and creep phases of the tests. Mean axial Lagrangian strains in the main *in vivo* loading direction and the perpendicular direction will be referred to as "strain in the MD" and "strain in the PD" from here on. For creep strain data, the initial strains upon reaching the creep load were subtracted from the total strain to represent strain due to creep. The strain versus time data for each specimen were curve-fit to the function αt^n using the least squares method in MATLAB (The MathWorks Inc., Natick, MA) where α is a material constant and n is the rate of creep. The goodness of fit was assessed using the R^2 coefficient of determination. The above analysis was performed for all $n = 15$ tested specimens.

For $n = 8$ specimens that yielded OCT data during both the pre-creep and creep loading phases of testing (see details below), nominal stresses in the MD and PD were calculated by normalizing the force data from the load cells by the cross-sectional areas that were perpendicular to each respective direction. Cross-sectional areas were calculated using thicknesses measured by OCT before the start of the pre-creep loading phase. The nominal stress values will be referred to as "stress in the MD" and "stress in the PD". Local values of major and minor principal strain angles were also extracted over the region of interest in the center of the specimens using the commercial DIC system. Relative frequency of major and minor principal strain values over the entire region of interest were computed, from 90° to −90° where 0° was the MD and 90° and −90° were both the PD, and they were compared at the same stress values in the PD.

2.4. OCT imaging and out-of-plane deformations

OCT was used to image the specimens in their through-thickness direction. As shown in Fig. 1(b), the objective lens of a custom 830 nm OCT probe was positioned above the sample focusing at its center. The OCT system was based on a conventional spectral domain design using a superluminescent diode light source (SLD; Superlum, Cork, Ireland; $\lambda = 837$ nm, $\Delta\lambda = 54$ nm) and a linescan camera-based spectrometer (AViiVA EM1; Teledyne, Milpitas, CA; 1024 pixel, 78 kHz). The 20 μm focused beam was 2D raster-scanned across the sample to generate tomographic images that were 5 × 5 mm^2 in lateral dimension and up to 2 mm in physical tissue depth. Each 3D image took approximately 4 s to acquire. To avoid optical crosstalk, the DIC cameras were outfitted with short pass filters (FES0650, Thorlabs Inc., Newton, NJ) to block the near infrared OCT light. Scans were taken before and after the pre-creep loading phase and during the creep loading phase of each test.

The OCT image processing followed the standard Fourier transform-based procedure (Leitgeb et al., 2003). For examining depth information, image cross-sections were taken from the volumetric data. Fig. 2(a) shows a representative OCT in-plane image, where the black spots were due to the presence of paint speckles and Fig. 2(b) shows an out-of-plane image with characteristic depth features. The black speckles in the OCT images were used in a template-matching procedure so as to track changes in thickness at the same location within the specimens. This was done since, as the specimens were biaxially loaded, they moved in-plane. To determine tissue thickness, the depth difference between the top and bottom interfaces of the tissue was calculated at one location during pre-creep and three locations during creep to obtain mean values for each specimen. A lateral moving average (0.4 × 0.4 mm^2) was used to improve the signal-to-noise ratio, particularly at the bottom interfaces, where contrast was reduced due to light attenuation through the tissue. The depth trace (intensity *vs.* depth) was then extracted at the locations of interest. Fig. 2(c) shows the depth trace and its derivative (slope), from which the depth locations of the top and bottom interfaces were determined as the local maxima and minima.

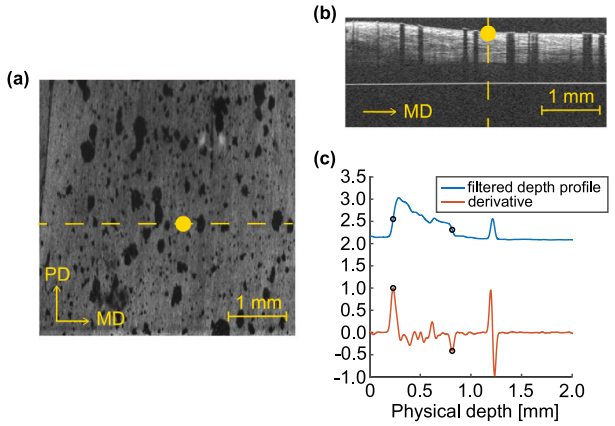

Fig. 2. (a) Representative in-plane image of one USL specimen. (b) Out-of-plane image at one marked location (yellow dotted line) in (a). (c) Filtered depth profile data and corresponding derivative at one marked location (yellow dotted line) in (b). Open circles indicate the locations of the top and bottom interfaces.

2.5. Statistical analysis

For comparison of the USLs in the MD and PD during pre-creep, strains were selected at equal values of stress (50 kPa, 100 kPa, and 150 kPa) for each specimen in their respective loading directions and compared using a paired Student's t-test. Similarly, for comparisons of the USLs in the MD and PD during creep, the parameters of the curve-fit function, n and α, were compared between the MD and PD using Student's t-tests. None of the assumptions for the statistical analysis were violated. All reported numerical values are presented as the mean ± the standard deviation. Statistical analyis was conducted using SPSS Statistics software (IBM SPSS Statistics, IBM Corp., Armonk, NY), and statistical significance was set to $p < 0.05$.

3. Results

The in-plane (Lagrangian and normal) strains were measured successfully in all USL specimens throughout the pre-creep and creep-loading phases of the testing protocol ($n = 15$). However, the changes in thickness of USL specimens were successfully computed only for a subset of specimens ($n = 8$). Thickness measurements were used to calculate the (nominal and normal) stresses in the MD and PD for each of these specimens during the pre-creep loading phase of the testing protocol.

The strain fields in both the MD and PD were highly heterogeneous across each tested specimen ($n = 15$), as shown in Fig. 3 for one representative specimen. For this specimen, the average (over the selected region of interest) strain in the PD was much higher than the average strain in the MD at stress values of 50 kPa and 150 kPa in the corresponding directions. As expected, the overall stress–strain curves in the MD and PD were found to be highly nonlinear, with an initial toe region followed by a more linear region (Fig. 4(a)–(b)). For some specimens (6 out of 8) the tissues appeared to be stiffer in the MD than in the PD, but for others (2 out of 8) the opposite trend was observed. However, when comparing the average strains across the tested specimens ($n = 8$), it was found that the average strain was significantly higher in the PD than in the MD at equivalent stress values of 50 kPa ($p = 0.036$), 100 kPa ($p = 0.025$), and 150 kPa ($p = 0.025$) (Fig. 4(c)).

The principal strains and principal directions of strains were also found to be heterogeneous, as shown in Fig. 5(a) for one representative specimen at stress values of 5 kPa, 50 kPa and 150 kPa in the PD. Fig. 5(a) shows that the directions of principal strain were different from the MD and PD, the axial loading directions. The principal directions of strains were computed at comparable stress values of 50 kPa and 150 kPa in the PD for $n = 8$ specimens, and the results are reported in Fig. 5(b). One can note that the maximum principal strains always occurred away from the MD (0 degree), which is the main *in vivo* loading direction. Moreover, the average maximum principal strain was more than double the average minimum principal strain over $n = 8$ specimens (Fig. 5(c)).

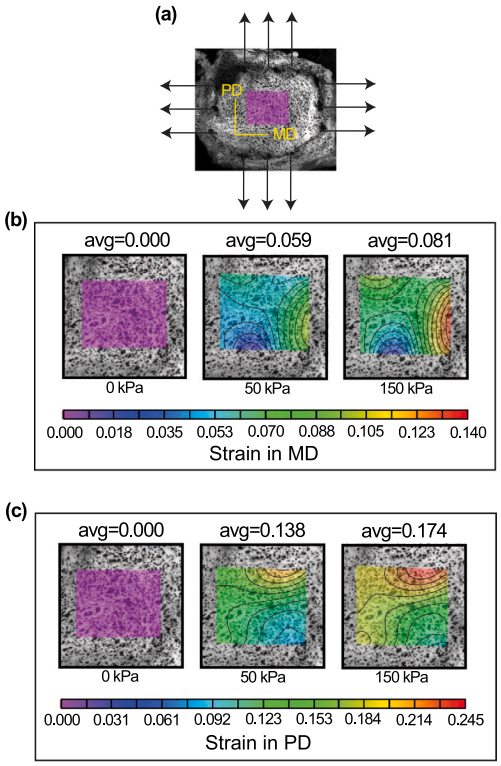

Fig. 3. (a) Representative specimen speckled for DIC strain measurement, with reported MD and PD aligned along the loading axes. (b) Map of (normal, Lagrangian) strains and corresponding average strains in the MD at (nominal) stress levels of 0 kPa, 50 kPa, and 150 kPa in the MD. (c) Map of (normal, Lagrangian) strains and average strains in the PD at (nominal) stress levels of 0 kPa, 50 kPa, and 150 kPa in the PD.

The strain fields during the creep phase of the testing protocol preserved the pre-creep heterogeneity, as demonstrated in Fig. 6. From Fig. 6, one can observe that the strain fields at the beginning ($t = 0$ s) and at the end of creep ($t = 2400$ s) for one representative specimen in either the MD or PD were comparable, with the average strains changing by no more than 0.01. The strain over time data for all the tested specimens ($n = 15$) are reported for the MD and PD in Fig. 7(a)–(b). The parameters n and α, which were used to capture the nonlinear creep response of the tested USL specimens in the MD and PD, were compared. The R^2 for each of the curve fit ranged from 0.875 to 0.994 with average values of 0.971 for the MD and 0.955 for the PD. The values of n ($p = 0.71$) and α ($p = 0.43$) were not statistically different between the MD and PD. This finding indicates that the creep behavior in the two loading directions was not statistically different (Fig. 7(c)).

OCT measurements provided a first look into the variation of thickness in USL specimens. During pre-creep loading, the reduction in thickness was consistent, as shown in Fig. 8 and reported in Table 1. During creep loading, the relative change in thickness over time was calculated at three locations to obtain a mean value for each USL specimen over time. As an example, Fig. 9(a) shows the relative thickness change over time calculated at three locations as well as their mean value over time. Although there was some variation, these relative changes in thickness were comparable, indicating that the relative change in thickness was consistent across each USL specimen. The mean

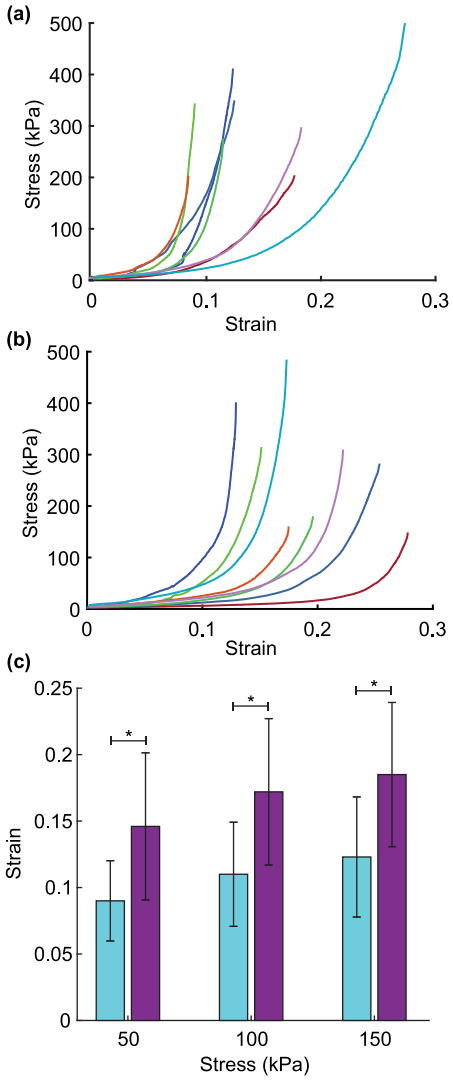

Fig. 4. Stress–strain curves in the (a) MD and (b) PD for a subset of tested specimens ($n = 8$). Data from the same specimen are reported using the same color. (c) Mean (± S.D.) strain in the MD (blue) and PD (purple) at equivalent stress levels of 50, 100, and 150 kPa in the MD and PD computed from $n = 8$ specimens. $*$, $p < 0.05$.

Table 1
In-plane strains and relative thickness change (%) for $n = 8$ specimens at the end of the pre-creep loading phase.

Specimens	Strain in MD	Strain in PD	Thickness change (%)
1	0.178	0.279	−32.2
2	0.131	0.118	−24.6
3	0.127	0.255	−37.8
4	0.095	0.152	−22.2
5	0.086	0.179	−17.2
6	0.098	0.246	−34.9
7	0.207	0.214	−27.1
8	0.261	0.194	−19.4

relative thickness change versus time data for each of $n = 8$ specimens are presented in Fig. 9(b). Interestingly, the relative thickness was found to increase, decrease, or remain almost unchanged during creep loading, in contrast to the consistent reduction during pre-creep loading.

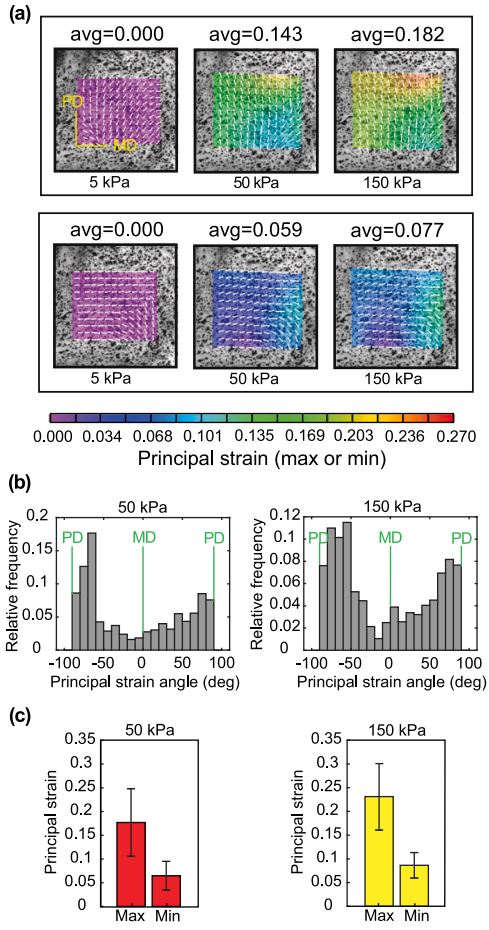

Fig. 5. (a) Maps of maximum (top row) and minimum (bottom row) principal strains and corresponding average principal strains at (nominal and normal) stress values of 5 kPa, 50 kPa, and 150 kPa in the PD for one representative specimen. Small white arrows denote the directions of maximum (top row) and minimum (bottom row) principal strains. (b) Relative frequency of max principal strain angles and (c) mean (±S.D.) of the maximum and minimum principal strains at stress values of 50 kPa and 150 kPa in the PD computed from $n = 8$ specimens.

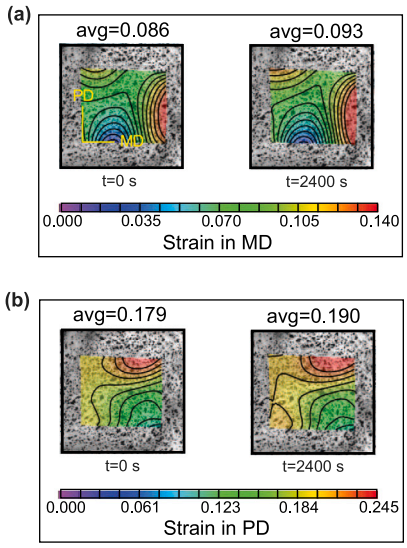

Fig. 6. Maps of (normal, Lagrangian) strains and corresponding average strains in the (a) MD and (b) PD for one specimen at the start ($t = 0$ s) and at the end ($t = 2400$ s) of creep.

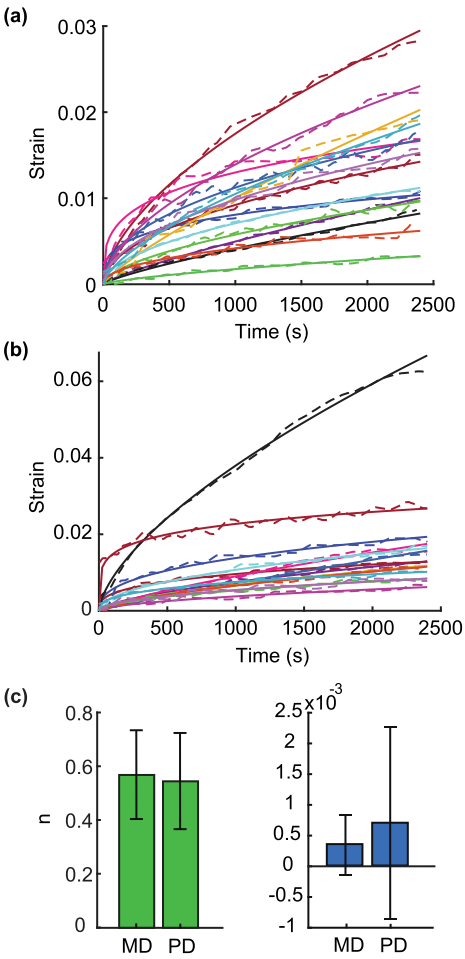

Fig. 7. Moving average (dashed lines) and curve fitting (continuous lines) of (normal, Lagrangian) strain over time during creep testing in the (a) MD and (b) PD for $n = 15$ specimens. Data from the same specimen are reported using the same color. (c) Mean (± S.D.) values of the parameters, n and α, in the equation αt^n used to fit the creep data from $n = 15$ specimens.

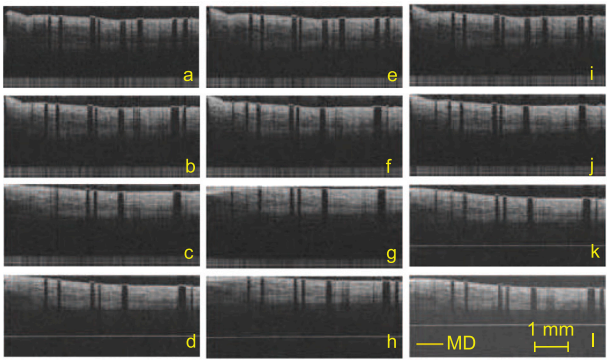

Fig. 8. Images of the cross-sections of one representative USL specimen during pre-creep subjected to stresses that increase from (a) 2.0 kPa in the MD and 1.8 kPa in the PD to (l) 198 kPa in the MD and 144 kPa in PD.

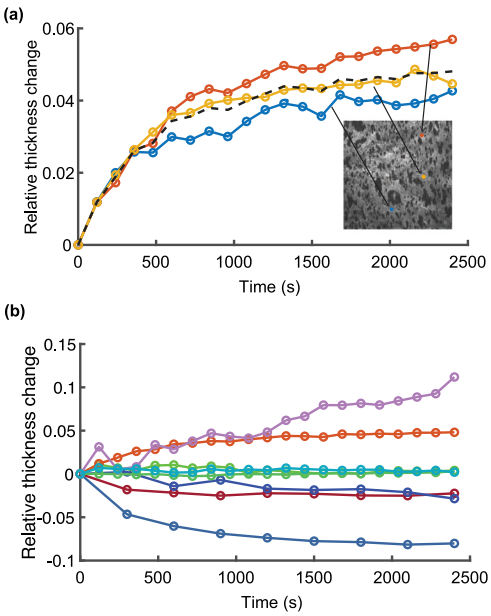

Fig. 9. (a) Relative thickness change over time during creep at three in-plane locations across one representative USL specimen, as shown in the inset, with the mean relative thickness change. (b) Mean relative thickness change over time during creep for $n = 8$ USL specimens.

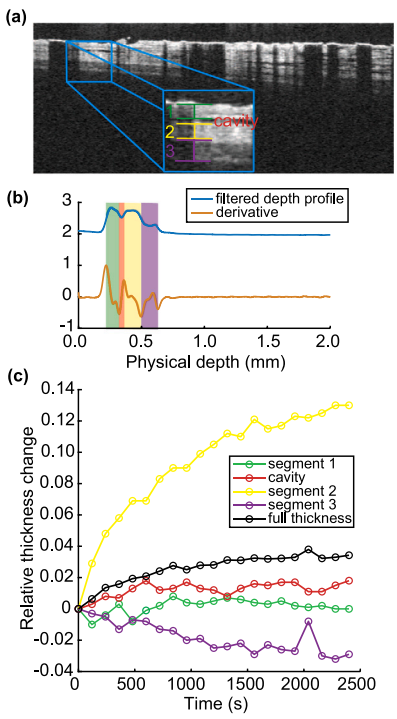

Fig. 10. (a) Cross-sectional image of one USL specimen showing three sublayers (segments 1, 2, and 3) and one cavity at the beginning of creep. (b) Filtered depth profile data and corresponding derivative, showing the presence of three sublayers and one cavity. (c) Relative thickness change of each sublayer and cavity in (a) and the full tissue over time during creep.

Discussion

This study reported the in-plane and out-of-plane deformations of gilt USLs during planar equibiaxial testing. The in-plane strains were found to be highly heterogeneous (Fig. 3), likely due to the complex organization of primary USL components: collagen, elastin, smooth muscle, nerves, blood vessels, and lymph vessels. Under increasing equibiaxial stresses, the gilt USLs strained significantly less and were significantly stiffer in the MD than the PD (Fig. 4(a)–(c)). These results agree well with findings reported by Baah-Dwomoh et al. (2016), where the sow USLs were also reported to be stiffer (although not

significantly stiffer) in the MD than the PD. To directly compare our data on gilt USLs to the data on sow USLs (Baah-Dwomoh et al., 2016), we calculated the mean secant moduli from the current stress–strain curves up to 95 kPa (Fig. 4(a)–(b)) and found them to be 986 ± 314 kPa for the MD and 670 ± 239 kPa for the PD. Using a Student's t-test, the gilt USLs were found to be significantly stiffer than the sow USLs (secant moduli reported in Baah-Dwomoh et al. (2016)) in the MD ($p = 0.002$). They were also stiffer in the PD, but due to high variance in the data from sow USLs, this result was not statistically significant ($p = 0.075$). Together these data suggest that the USLs in sows may be more compliant, likely due to the extreme loading and deformations that they experience supporting the gravid uterine horns during pregnancy.

The in-plane angles of maximum principal strains were closer to the angle defining the PD throughout testing and, consequently, the in-plane angles of minimum principal strains were closer to the angle defining the MD, as exemplified by the representative specimen in Fig. 5(a). The frequency of the angles of maximum principal strains at 90° and −90°, or exactly in the PD, was quite high while the frequency of such angles at 0°, or in the MD, and in other directions was much lower (Fig. 5(b)). It is very likely that more collagen fibers were oriented in the MD before testing began and, due to the constraints imposed by the clamping method (i.e., the edges of the specimens were not able to expand freely in the lateral directions within the clamps), the collagen fibers could not re-orient during testing. Therefore, the in-plane angles of principal strains did not change as the stresses increased (Fig. 5(b)). Among other things, these results seem to confirm that we performed planar biaxial testing along the material axes of the USLs.

The patterns of heterogeneous in-plane strains in the gilt USLs were maintained throughout creep testing, as demonstrated in Fig. 6. Local regions with high (low) strains continued to experience high (low) strains over the duration of creep. Although all the gilt USLs strained over time under constant equibiaxial loading, no specimen, except for one, experienced an increase in strain higher than 3% in either the MD or PD (Fig. 7(a)–(b)). The study published by Baah-Dwomoh et al. (2018) showed that sow USLs also experienced similar levels of creep. While these findings provide some insight into the contribution of viscoelasticity to the mechanical properties of the gilt USLs, how such time-dependent properties are altered by different physiologic and pathophysiologic conditions remains to be investigated.

A simple power law model was used to curve-fit the creep data from all specimens in each of the two loading directions, the MD and PD (Fig. 7), similarly to Provenzano et al. (2001) and Hingorani et al.'s (2004) uniaxial creep curve fitting of rat and rabbit medial collateral ligaments, respectively. This was done solely to compare the creep behavior between the MD and PD. Neither of the model parameters, the coefficient α or the creep rate n, were statistically different between the MD and the PD, though there was much more variability in the α values, especially in the PD (Fig. 7(c)). Such variability is to be expected since the values of α and n were computed by fitting creep data that were collected at comparable yet different equibiaxial loads/stresses from 15 specimens. The large variability of the model parameters may suggest some potential non-linearity in the viscoelastic behavior of the USLs. However, future creep experiments should be conducted at significantly different load/stress levels to determine whether the creep rate changes with load/stress level or whether such rate is independent of the load/stress level. Unfortunately, we could not increase the applied equibiaxial loads in this study as higher loads caused specimen breakage. We also did not want to further lower the loads since loads lower than 1 N would be more than one order of magnitude lower than the loads measured *in vivo* (Smith et al., 2013; Luo et al., 2014).

In this study, seven specimens were taken from the distal regions of the swine USLs, five specimens were taken from the intermediate regions, and three specimens were taken from the proximal regions. Fewer specimens were collected from the proximal regions due to difficulties with dissecting large portions of the USLs adjacent to the sacral spine. Large variation in tissue structure and content from one USL specimen to the other resulted in differences in the value of the applied equibiaxial loading during creep. After some mechanical tests, it became apparent that not all of the USL specimens could withstand an equibiaxial load of 2 N, and the applied equibiaxial load was lowered to 1.5 N and eventually 1 N to avoid failure of the specimens before the start of creep testing. Due to the microstructural variations between the three regions of the USLs, one would expect the mechanical properties to vary between the regions, i.e. the loosely-organized, collagen-rich sacral region may be expected to be more compliant than the tightly-organized, smooth muscle-dominated cervical region (Donaldson et al., 2021). However, there were no apparent regional differences in the preliminary data, and there were not enough specimens tested per region to perform statistical analysis with enough power to be meaningful. Large variation in structure within a single animal (or a human) and between several animals (or humans) is a typical characteristic of the USLs. Several anatomical studies report differences in the locations, connection points, and sizes of the USLs with the ligaments being indistinguishable in some patients (Campbell, 1950; Buller et al., 2001; Umek et al., 2004; Ramanah et al., 2012; Donaldson et al., 2021).

The OCT was successfully used to measure the out-of-plane deformations in a subset of USL specimens. The other specimens were mostly of greater thickness, making the visualization of the bottom surface of the tissue challenging due to light attenuation. This difficulty can be mitigated in future studies by using a light source with a longer wavelength for higher penetration depth or by implementing dual imaging heads to monitor both the top and bottom of the specimens and effectively double the penetration depth. Other factors, such as preloading-induced movement and water surface reflection, may have also compromised the imaging in some cases. But, despite the limitations, this preliminary investigation has shown that OCT has the potential to complement other mechanical characterization methods in a significant way. Direct thickness monitoring, as shown in Fig. 8, adds another dimension to the traditional in-plane mechanical testing and provides a more complete picture of the mechanical function of USLs. There was a clear correlation between in-plane strain increase and thickness decrease (Table 1) during pre-creep loading. However, no apparent correlation was observed during creep loading, where the in-plane strains continued to increase for all specimens yet the changes in thickness, which were also inhomogeneous (Fig. 9(a)), were not consistent across the specimens (Fig. 9(b)). The complex internal structure of the USLs may be responsible for the through-thickness behavior of the USLs, possibly favoring hydration and dehydration during testing. Even for thickness beyond OCT's capability, imaging of partial tissue depth may provide useful information. Using the OCT, we were able to observe the internal morphology of USL specimens, such as the presence of sublayers and internal cavities. An example of different structural features, including three sublayers and a small cavity, in one USL specimen is shown in Fig. 10. The thickness of these features was independently tracked and both an increase and a decrease in relative thickness were observed, while the total relative thickness of the specimen was found to increase. Fig. 10 demonstrates the depth-dependent heterogeneity of the USLs, even at the same in-plane location. Overall, our findings indicate that OCT-based probes could be used to evaluate regional differences across the whole USL and variation across subjects *in vivo*.

No experimental studies have been published on how the mechanical properties of the USLs change with pregnancy, aging, or prolapse in an animal model. To determine how such properties may be altered, *in vivo* longitudinal studies must be conducted and, for such studies, non-invasive testing techniques need to be developed. The outcome of this research could guide the development of new tools (e.g., mechanics-based or OCT-based probes) to test the integrity of USLs *in vivo*, without sacrificing the animals. Some *in vivo* techniques have been developed and adopted in patients undergoing pelvic surgery by Smith et al. (2013). These authors determined the force–displacement behavior and

stiffness of uterine suspensory tissue, which includes the USLs, the cardinal ligaments, and other contiguous supportive tissues. The same techniques were used by Luo et al. (2014) to assess the time-dependent force–displacement behavior of the same tissue complex. However, these measurements were performed over a short time interval (60 s) while the patients were undergoing pelvic surgery.

The USLs are the most frequently used native tissues for surgical suspension of the prolapsed pelvic organs. Several procedures for POP treatment exist that target the USLs, including variations on securing the prolapsed vagina or uterus to the USLs *via* suture repair. Moreover, transvaginal prolapse repair meshes have been banned because of high rates of complications associated with these procedures, including mesh exposure, mesh erosion, pelvic pain, and dyspareunia (Dietz et al., 2003; Jones et al., 2009; Liang et al., 2013). New mesh materials that are mechanically similar to the tissues they are to enhance or replace need to be created. The first step toward this goal is to characterize the mechanical properties of the tissues in women without POP.

4. Conclusion

This study presents the first quantification of in-plane and out-of plane deformations of gilt USLs subjected to biaxial loading. Deformations were measured by integrating DIC and OCT methods with a custom-built planar biaxial testing device. The results suggest that the USL specimens deformed quasi-statically more in the PD than in the MD as the equibiaxial loading slowly increased, while the thickness consistently decreased. However, under constant equibiaxial loading, the increase of in-plane strain over time was comparable in the PD and MD but variability in the out-of-plane deformations over time was observed, with some USL specimens decreasing in thickness and others increasing. Future mechanical experiments will need to account for the heterogeneity of the USLs, as revealed using the proposed methods, to determine their *in vivo* support function.

CRediT authorship contribution statement

Kandace Donaldson: Conceptualization, Methodology, Software, Validation, Formal analysis, Investigation, Data curation, Writing – original draft. **Joseph Thomas:** Methodology, Software, Validation, Formal analysis, Investigation, Data curation, Writing – original draft. **Yizheng Zhu:** Conceptualization, Resources, Writing – original draft, Writing – review & editing, Supervision, Project administration, Funding acquisition. **Sherrie Clark-Deener:** Methodology, Resources, Writing – review & editing. **Marianna Alperin:** Conceptualization, Methodology, Writing – review & editing. **Raffaella De Vita:** Conceptualization, Methodology, Resources, Writing – original draft, Writing – review & editing, Visualization, Supervision, Project administration, Funding acquisition.

Declaration of competing interest

The authors declare the following financial interests/personal relationships which may be considered as potential competing interests: Raffaella De Vita reports financial support was provided by National Science Foundation.

Acknowledgments

Funding was provided by National Science Foundation Grant No. 1804432. The authors would like to thank Talia Baddour for assistance with mechanical data collection and analysis.

References

Adhi, M., Duker, J.S., 2013. Optical coherence tomography – current and future applications. Curr. Opin. Ophthalmol. 24 (3), 213–221.
Baah-Dwomoh, A., Alperin, M., Cook, M., De Vita, R., 2018. Mechanical analysis of the uterosacral ligament: Swine vs. human. Ann. Biomed. Eng. 46 (12), 2036–2047.
Baah-Dwomoh, A., McGuire, J., Tan, T., De Vita, R., 2016. Mechanical properties of female reproductive organs and supporting connective tissues: A review of the current state of knowledge. Appl. Mech. Rev. 68 (6).
Barber, M.D., Maher, C., 2013a. Apical prolapse. Int. Urogynecol. J. 24 (11), 1815–1833.
Barber, M.D., Maher, C., 2013b. Epidemiology and outcome assessment of pelvic organ prolapse. Int. Urogynecol. J. 24 (11), 1783–1790.
Barber, M.D., Visco, A.G., Weidner, A.C., Amundsen, C.L., Bump, R.C., 2000. Bilateral uterosacral ligament vaginal vault suspension with site-specific endopelvic fascia defect repair for treatment of pelvic organ prolapse. Am. J. Obstet. Gynecol. 183 (6), 1402–1411.
Becker, W., De Vita, R., 2015. Biaxial mechanical properties of swine uterosacral and cardinal ligaments. Biomech. Model. Mechanobiol. 14 (3), 549–560.
Bouma, B.E., Tearney, G.J., Compton, C.C., Nishioka, N.S., 2000. High-resolution imaging of the human esophagus and stomach in vivo using optical coherence tomography. Gastrointest. Endosc. 51 (4 Pt 1), 467–474.
Buller, J.L., Thompson, J.R., Cundiff, G.W., Sullivan, L.K., Ybarra, M.A.S., Bent, A.E., 2001. Uterosacral ligament: Description of anatomic relationships to optimize surgical safety. Obstet. Gynecol. 97 (6), 873–879.
Campbell, R.M., 1950. The anatomy and histology of the sacrouterine ligaments. Am. J. Obstet. Gynecol. 59 (1), 1–12.
Chao, F.L., Rosamilia, A., Dwyer, P.L., Polyakov, A., Schierlitz, L., Agnew, G., 2012. Does pre-operative traction on the cervix approximate intra-operative uterine prolapse? A randomised controlled trial. Int. Urogynecol. J. 23 (4), 417–422.
Danso, E.K., Schuster, J.D., Johnson, I., Harville, E.W., Buckner, L.R., Desrosiers, L., Knoepp, L.R., Miller, K.S., 2020. Comparison of biaxial biomechanical properties of post-menopausal human prolapsed and non-prolapsed uterosacral ligament. Sci. Rep. 10 (1), 1–14.
Dietz, H.P., Vancaillie, P., Svehla, M., Walsh, W., Steensma, A.B., Vancaillie, T.G., 2003. Mechanical properties of urogynecologic implant materials. Int. Urogynecol. J. 14 (4), 239–243.
Diwadkar, G.B., Barber, M.D., Feiner, B., Maher, C., Jelovsek, J.E., 2009. Complication and reoperation rates after apical vaginal prolapse surgical repair: A systematic review. Obstet. Gynecol. 113 (2), 367–373.
Donaldson, K., Huntington, A., De Vita, R., 2021. Mechanics of uterosacral ligaments: Current knowledge, existing gaps, and future directions. Ann. Biomed. Eng. 49 (8), 1788–1804.
Doumouchtsis, S.K., Gauthaman, N., Khunda, A., Basu, M., Dadhwal, K., Gayle, Y.V., Durnea, C.M., 2017. Comparison between the valsalva maneuver and intraoperative traction measurements in pelvic organ prolapse assessment. Int. J. Gynecol. Obstet. 139 (3), 358–362.
Drexler, W., Fujimoto, J.G., 2008. State-of-the-art retinal optical coherence tomography. Prog. Retin. Eye Res. 27 (1), 45–88.
Fayyad, A., Hill, S., Gurung, V., Prashar, S., Smith, A.R.B., 2007. How accurate is symptomatic and clinical evaluation of prolapse prior to surgical repair? Int. Urogynecol. J. 18 (10), 1179–1183.
Fercher, A.F., Drexler, W., Hitzenberger, C.K., Lasser, T., 2003. Optical coherence tomography - principles and applications. Rep. Progr. Phys. 66 (2), 239–303, publisher: IOP Publishing.
Hingorani, R.V., Provenzano, P.P., Lakes, R.S., Escarcega, A., Vanderby, R., 2004. Nonlinear viscoelasticity in rabbit medial collateral ligament. Ann. Biomed. Eng. 32 (2), 306–312.
Holt, E., 2019. US FDA rules manufacturers to stop selling mesh devices. Lancet 393 (10182), 1686.
Huang, D., Swanson, E.A., Lin, C.P., Schuman, J.S., Stinson, W.G., Chang, W., Hee, M.R., Flotte, T., Gregory, K., Puliafito, C.A., Fujimoto, J.G., 1991. Optical coherence tomography. Science 254 (5035), 1178–1181, publisher: American Association for the Advancement of Science.
Huang, Y.P., Zheng, Y.P., Wang, S.Z., Chen, Z.P., Huang, Q.H., He, Y.H., 2009. An optical coherence tomography (OCT)-based air jet indentation system for measuring the mechanical properties of soft tissues. Meas. Sci. Technol. 20 (1), 015805.
Huntington, A., Abramowitch, S.D., Moalli, P.A., De Vita, R., 2021. Strains induced in the vagina by smooth muscle contractions. Acta Biomater. 129, 178–187.
Huntington, A., Rizzuto, E., Abramowitch, S.D., Del Prete, Z., De Vita, R., 2019. Anisotropy of the passive and active rat vagina under biaxial loading. Ann. Biomed. Eng. 47 (1), 272–281.
Jang, I.-K., Tearney, G.J., MacNeill, B., Takano, M., Moselewski, F., Iftima, N., Shishkov, M., Houser, S., Aretz, H.T., Halpern, E.F., Bouma, B.E., 2005. In vivo characterization of coronary atherosclerotic plaque by use of optical coherence tomography. Circulation 111 (12), 1551–1555.
Jones, K.A., Feola, A., Meyn, L., Abramowitch, S.D., Moalli, P.A., 2009. Tensile properties of commonly used prolapse meshes. Int. Urogynecol. J. 20 (7), 847–853.
Larin, K.V., Sampson, D.D., 2017. Optical coherence elastography – OCT at work in tissue biomechanics [Invited]. Biomed. Opt. Express 8 (2), 1172–1202.

Leitgeb, R., Hitzenberger, C., Fercher, A., 2003. Performance of fourier domain vs time domain optical coherence tomography. Opt. Express 11 (8), 889.

Liang, R., Abramowitch, S., Knight, K., Palcsey, S., Nolfi, A., Feola, A., Stein, S., Moalli, P.A., 2013. Vaginal degeneration following implantation of synthetic mesh with increased stiffness. BJOG 120 (2), 233–243.

Luo, J., Smith, T.M., Ashton-Miller, J.A., DeLancey, J.O.L., 2014. In vivo properties of uterine suspensory tissue in pelvic organ prolapse. J. Biomech. Eng. 136 (2).

Margulies, R.U., Rogers, M.A.M., Morgan, D.M., 2010. Outcomes of transvaginal uterosacral ligament suspension: Systematic review and metaanalysis. Am. J. Obstet. Gynecol. 202 (2), 124–134.

Matveev, L.A., Karashtin, D.A., Sovetsky, A.A., Gubarkova, E.V., Sirotkina, M.A., Matveyev, A.L., Shabanov, D.V., Gelikonov, G.V., Gelikonov, V.M., Druzhkova, I.N., Gladkova, N.D., Vitkin, A., Zagaynova, E.V., Zaitsev, V.Y., 2017. Quasistatic in-depth local strain relaxation/creep rate mapping using phase-sensitive optical coherence tomography. In: Optical Coherence Imaging Techniques and Imaging in Scattering Media II, Vol. 10416. SPIE, pp. 109–114.

Pack, E., Stewart, J., Rhoads, M., Knight, J., Clark, S., Schmale III, D.G., De Vita, R., 2020. Effects of short-term moderate ZEN consumption on uterosacral ligament elasticity in pubertal gilts. Res. Vet. Sci. 133, 202–209.

Provenzano, P., Lakes, R., Keenan, T., Vanderby, R., 2001. Nonlinear ligament viscoelasticity. Ann. Biomed. Eng. 29 (10), 908–914.

Ramanah, R., Berger, M.B., Parratte, B.M., DeLancey, J.O.L., 2012. Anatomy and histology of apical support: A literature review concerning cardinal and uterosacral ligaments. Int. Urogynecol. J. 23 (11), 1483–1494.

Siddique, S.A., Gutman, R.E., Ybarra, M.A.S., Rojas, F., Handa, V.L., 2006. Relationship of the uterosacral ligament to the sacral plexus and to the pudendal nerve. Int. Urogynecol. J. 17 (6), 642–645.

Skoczylas, L.C., Turner, L.C., Wang, L., Winger, D.G., Shepherd, J.P., 2014. Changes in prolapse surgery trends relative to FDA notifications regarding vaginal mesh. Int. Urogynecol. J. 25 (4), 471–477.

Smith, T.M., Luo, J., Hsu, Y., Ashton-Miller, J., DeLancey, J.O.L., 2013. A novel technique to measure in vivo uterine suspensory ligament stiffness. Am. J. Obstet. Gynecol. 209 (5), 484–e1.

Sun, C., Standish, B., Vuong, B., Wen, X.Y., Yang, V., 2013. Digital image correlation–based optical coherence elastography. J. Biomed. Opt. 18 (12), 121515.

Sun, C., Standish, B., Yang, V.X., 2011. Optical coherence elastography: current status and future applications. J. Biomed. Opt. 16 (4), 043001.

Sutton, M.A., Orteu, J., Schreier, H., 2009. Image Correlation for Shape, Motion and Deformation Measurements. Springer.

Tan, T., Cholewa, N.M., Case, S.W., De Vita, R., 2016. Micro-structural and biaxial creep properties of the swine uterosacral–cardinal ligament complex. Ann. Biomed. Eng. 44 (11), 3225–3237.

Turner, L.C., Lavelle, E.S., Shepherd, J.P., 2016. Comparison of complications and prolapse recurrence between laparoscopic and vaginal uterosacral ligament suspension for the treatment of vaginal prolapse. Int. Urogynecol. J. 27 (5), 797–803.

Umek, W.H., Morgan, D.M., Ashton-Miller, J.A., DeLancey, J.O.L., 2004. Quantitative analysis of uterosacral ligament origin and insertion points by magnetic resonance imaging. Obstet. Gynecol. 103 (3), 447.

Vierhout, M.E., Stoutjesdijk, J., Spruijt, J., 2006. A comparison of preoperative and intraoperative evaluation of patients undergoing pelvic reconstructive surgery for pelvic organ prolapse using the pelvic organ prolapse quantification system. Int. Urogynecol. J. 17 (1), 46–49.

Vineyard, D.D., Kuehl, T.J., Coates, K.W., Shull, B.L., 2002. A comparison of preoperative and intraoperative evaluations for patients who undergo site-specific operation for the correction of pelvic organ prolapse. Am. J. Obstet. Gynecol. 186 (6), 1155–1159.

Vu, D., Haylen, B.T., Tse, K., Farnsworth, A., 2010. Surgical anatomy of the uterosacral ligament. Int. Urogynecol. J. 21 (9), 1123–1128.

Wu, J.M., Hundley, A.F., Fulton, R.G., Myers, E.R., 2009. Forecasting the prevalence of pelvic floor disorders in US women: 2010 to 2050. Obstet. Gynecol. 114 (6), 1278–1283.

Wu, J.M., Matthews, C.A., Conover, M.M., Pate, V., Funk, M.J., 2014. Lifetime risk of stress incontinence or pelvic organ prolapse surgery. Obstet. Gynecol. 123 (6), 1201.